Measuring Spectral Actinic Flux and Irradiance: Experimental Results from the Actinic Flux Determination from Measurements of Irradiance (ADMIRA) Project

A. R. WEBB,* A. F. BAIS,+ M. BLUMTHALER,# G-P. GOBBI,@ A. KYLLING,& R. SCHMITT,** S. THIEL,++ F. BARNABA,@ T. DANIELSEN,& W. JUNKERMANN,++ A. KAZANTZIDIS,+ P. KELLY,* R. KIFT,* G. L. LIBERTI,@ M. MISSLBECK,++ B. SCHALLHART,# J. SCHREDER,# AND C. TOPALOGLOU+

*Department of Physics, University of Manchester Institute of Science and Technology, Manchester, United Kingdom
+Aristotle University of Thessaloniki, Laboratory of Atmospheric Physics, Thessaloniki, Greece
#Institute for Medical Physics, University of Innsbruck, Innsbruck, Austria
@Institute of Atmospheric Physics, CNR, Rome, Italy
&Norwegian Institute for Air Research, Kjeller, Norway
**Meteorologie Consult GmbH, Glashutten, Germany
++Fraunhofer Institute for Atmospheric Research, Garmisch-Partenkirchen, Germany

(Manuscript received 11 June 2001, in final form 31 October 2001)

ABSTRACT

Results are presented from the Actinic Flux Determination from Measurements of Irradiance (ADMIRA) campaign to measure spectral global UV irradiance and actinic flux at the ground, beneath an atmosphere well defined by supporting measurements. Actinic flux is required to calculate photolysis rates for atmospheric chemistry, yet most spectral UV measurements are of irradiance. This work represents the first part of a project to provide algorithms for converting irradiances to actinic fluxes with specified uncertainties. The campaign took place in northern Greece in August 2000 and provided an intercomparison of UV spectroradiometers measuring different radiation parameters, as well as a comprehensive radiation and atmospheric dataset. The independently calibrated spectroradiometers measuring irradiance and actinic flux agreed to within 5%, while measurements of spectral direct irradiance differed by 9%. Relative agreement for all parameters proved to be very stable during the campaign. A polarization problem in the Brewer spectrophotometer was identified as a problem in making radiance distribution measurements with this instrument. At UV wavelengths actinic fluxes F were always greater than the corresponding irradiance E by a factor between 1.4 and 2.6. The value of the ratio $F:E$ depended on wavelength, solar zenith angle, and the optical properties of the atmosphere. Both the wavelength and solar zenith angle dependency of the ratio decreased when the scattering in the atmosphere increased and the direct beam proportion of global irradiance decreased, as expected. Two contrasting days, one clear and one with higher aerosol and some cloud, are compared to illustrate behavior of the $F:E$ ratio.

1. Introduction

Ultraviolet (UV) radiation is a significant driver of atmospheric chemistry, since photodissociation of several important species occurs at these wavelengths. For example, the photolysis rates of ozone and nitrogen dioxide (NO_2) depend directly on the actinic fluxes (defined below) in the wavelength ranges responsible for these reactions [roughly UVB (280–315 nm) and UVA (315–400 nm), respectively]. Atmospheric chemistry calculations, or interpretation of experimental results, therefore require a knowledge of actinic fluxes, ideally as vertical profiles and with good spectral resolution so that any required photolysis rate can be calculated. Alternatively, photolysis rates can be measured directly with chemical actinometers, but this requires one instrument per species and lacks the versatility of the radiation measurements.

Spectral UV radiation measurements, while not commonplace, have become more readily available in the past decade. However, the vast majority of such data refers to spectral irradiance, that is, the radiation incident on a flat (usually horizontal) surface, that is, the radiance weighted with the cosine of the angle between the incident direction and the normal to the surface, and integrated over a hemisphere:

$$E(\lambda) = \int_0^{2\pi} \int_0^{\pi/2} L(\lambda, \theta, \phi) \cos\theta \sin\theta \, d\theta \, d\phi,$$

where $E(\lambda)$ is global irradiance at a specified wavelength, L is radiance, and θ and ϕ are zenith and azimuth angles, respectively. Calculating photolysis rates in atmospheric chemistry requires actinic flux

Corresponding author address: Dr. Ann R. Webb, Department of Physics, University of Manchester Institute of Science and Technology, P.O. Box 88, Manchester M60 1QD, United Kingdom.
E-mail: ann.webb@umist.ac.uk

$$F(\lambda) = \int_0^{2\pi} \int_{-\pi/2}^{\pi/2} L(\lambda, \theta, \phi) \sin\theta \, d\theta \, d\phi.$$

This is the radiation incident at a point (or on a very small sphere), that is, the unweighted radiance integrated over a sphere (Madronich 1987b).

A few direct measurements of spectral actinic fluxes have been reported (Shetter and Mueller 1999; Hofzumahaus et al. 1999, 2002), but the increasing number of UV monitoring sites measure irradiance, and some of them now have datasets that exceed 10 years in duration. Thus, a robust method of converting from irradiance measurements to actinic fluxes with known errors would provide archives of actinic fluxes and extend the use of existing UV irradiance monitoring stations. Since the radiance distribution $L(\lambda, \theta, \phi)$ depends on the scattering that takes place throughout the atmosphere, and thus on the three-dimensional atmospheric composition plus the surface properties, it is necessary to measure (or assume) the state of the atmosphere in the vertical when undertaking the E to F conversion.

The basic theory of the transfer from flat to spherical receiving surface was discussed by Madronich (1987a) and Van Weele et al. (1995). Broadband measurements were first used to develop empirical relationships between irradiances and actinic fluxes (Nader and White 1969; Madronich 1987a; Van Weele et al. 1995). Limitations imposed by the spectral weighting functions of the broadband instruments were avoided in more recent studies by Kazadzis et al (2000) and McKenzie et al. (2001), since both used spectrally resolved measurements. Kazadzis et al. compared spectral irradiance measurements with actinic flux calculations for clear sky conditions and showed that the isotropic assumption for diffuse radiation led to overestimates of actinic fluxes in polluted conditions. McKenzie et al. (2001) measured both irradiance and actinic flux over a 4-day period at an elevated, comparatively clean site. They found that with clear skies photolysis rates of ozone and NO_2 could be assessed from irradiance measurements for an additional uncertainty of less than 10%. Under cloudy conditions the uncertainties increased to 20% for ozone and even more for NO_2. As in the study by Kazadzis, it was the assumption of isotropy in the conversion that resulted in discrepancies in the cloudy situations. McKenzie et al. concluded that irradiance to actinic flux conversion factors depend on many variables, including solar zenith angle (SZA), aerosol optical depth, and cloud cover. The potential exists to use historical records of irradiances to increase knowledge of photolysis rates at the surface, but further study is needed to determine the errors involved in the conversions under different conditions.

This campaign was undertaken as part of the Actinic Flux Determination from Measurements of Irradiance (ADMIRA) project, part of the Fifth Framework Programme of the European Community. The aim of the project is to develop algorithms, with associated uncertainties, to enable the conversion of UV spectral global irradiance measurements into spectral actinic fluxes. The uncertainty associated with the conversion process depends to a large extent on the additional information available about the atmosphere at the time the irradiance measurements are made. In the worst case there is no additional information. Approaches that can be taken toward developing the algorithms are empirical and model-based. Both methods need a comprehensive set of measurements as a starting point. Here we describe the results from the initial ADMIRA campaign. It was designed to give high quality irradiance and actinic flux data together with additional information describing the optical properties of the sky. Since both irradiance and actinic flux change rapidly with, and are sensitive in different ways to, changing atmospheric conditions (e.g., cloud cover), it was important to carefully synchronize all the radiation measurements and, where possible, other data collection. Herein the dataset is described and used to illustrate what it teaches us about UV spectral irradiances and actinic fluxes. Further datasets will be gathered under a range of different climatologies during the rest of the project.

2. Site and instrumentation

The campaign took place in August 2000 at Nea Michaniona in northern Greece, at a site previously used for a large instrument intercomparison (Bais et al. 2001). The instruments were located on a flat roof (44 m east–west by 9 m north–south) in a coastal complex, with an instrument altitude of approximately 30 m above sea level. The geographical position was 40°28′N, 22°51′E. To the south was a sea horizon of at least 20 km, while on the landward side no elevations above the flat horizon caused significant obstruction to the instrument's field of view. The radiation instruments were mounted on the eastern half of the roof, while the supporting instrumentation was placed on the western roof. To the northern side of the building was a large courtyard where a mobile unit housing the Vehicle-Mounted Lidar System (VELIS) was parked.

The core spectral radiation measurements were made with a set of five scanning spectroradiometers. All the spectroradiometers were double monochromators with photomultiplier tube detectors. Their slit widths were in the range 0.5–1.0 nm full width half maximum (FWHM), and wavelength alignment was generally better than 0.05 nm. Each instrument was used for a number of different measurement tasks during the campaign, to maximize the information collected and minimize the risks of losing any one type of radiation measurement in the event of instrument malfunction. Table 1 lists the instruments and the tasks they undertook during the campaign.

The preliminary phase of the campaign allowed for the calibration and installation of the five spectroradi-

TABLE 1. The UV spectroradiometers and their measurement configurations used during the campaign.

Instrument*	Wavelength range (nm)	Global	Actinic	Direct	Radiance distribution	Global check	Actinic check	Min time step
UMIST Behtham DTM300	290–500	X	X			X	X	1 s
IFU Bentham DTM300	290–420	X	X			X	X	2 s
UIIMP Bentham DTM300	290–500			X	X	X		1 s
Brewer Mark III	290–365			X	X	X		3 s
CVI laser 110 mm	290–500		X				X	1 s

* Instruments of identical make are identified by their operators: UMIST = University of Manchester Institute of Science and Technology, IFU = Fraunhofer Institute, UIIMP = University of Innsbruck Institute of Medical Physics.

ometers on the roof. Calibrations for both irradiance and actinic flux are made by reference to standard lamps held by each institute and traceable through one or more transfers to one of the national standards laboratories. The lamps must be used at a fixed distance, which is simple to determine for the irradiance measurements. For the actinic flux heads the reference plane had been previously determined by using the inverse square law. The uncertainty of the actinic flux calibrations is therefore similar to those for irradiance, with a slight increase in uncertainty due to the experimental determination of the reference plane. With the exception of the Brewer, all instruments were temperature stabilized and used fiber-optic guides between the input optics and the entrance ports to the spectroradiometers. The three Bentham instruments each had two selectable entrance ports, and thus two fibers and two sets of input optics. Each had a cosine response head for global (downwelling) irradiance measurement, as well as either a 2π head (i.e., measuring over 2π steradians) for actinic flux, or a 1.5° field-of-view optic on a tracker for direct irradiance and radiance distribution measurements. The optic heads were all mounted at 1.3 m above the roof and arranged so as to avoid shadowing or obstruction of any of the fields of view. This was particularly important for the 2π heads that give as much weighting to radiation from the horizon as radiation from the zenith. Actinic flux measurements of the upper hemisphere (2π) performed near the surface of the earth should be nearly equal to the full 4π steradian measurements if the albedo is low. In a highly reflective environment (e.g., snow) or with the sensors at a significant distance above the surface, this assumption would not hold.

The angular response of the three actinic heads [Meteorologie Consult GmbH, Glashutten, Germany (METCON)] had previously been measured in the laboratory at the University of Innsbruck Institute for Medical Physics (UIIMP) in Austria. They all deviated less than 5% from the ideal flat response at all wavelengths for angles $<80°$ (Fig. 1). The observed slight azimuthal dependencies of three of the heads were estimated to give an uncertainty of no more than 3% in an actinic flux measurement. During field measurements the actinic flux heads were operated with a horizon ring around the base of the head to prevent any upwelling radiation from reaching the head (giving an effective angular response of zero for angles $>90°$), but this band could not be used during the laboratory characterizations. The three Bentham instruments had near-perfect cosine responses, though minor corrections were still made to the Fraunhofer Institute for Atmospheric Research (IFU) measurements during postprocessing of the irradiance measurements. The cosine response of the Brewer instrument is less perfect, though well defined, and cosine corrections are again made during postprocessing (ranging between 3.3% and 6.8%, depending on SZA and wavelength). The cosine-correction methods require the spatial distribution of radiation, usually derived from a model or assumed to be isotropic.

Two days of intercomparison followed the installation. These were designed to ascertain that all the instruments were measuring to the same absolute standard and were stable with respect to each other, before allocating each instrument to measure a different parameter. On the first day the four instruments that could measure global irradiance made synchronized measurements throughout the day from 290–500 nm (or the longest available wavelength), at 0.5-nm steps with 3 seconds per step, achieving agreement within $\pm 4\%$. On the second day the three instruments that could make actinic flux measurements followed a similar program, using the actinic heads, but with quicker scans of 2 seconds per step. Agreement was similar to that of the irradiance measurements. The remaining two instruments made alternating radiance distribution and synchronized direct irradiance measurements. The radiance distribution measurements were made at wavelengths 310.1 and 343.3 nm by the Brewer, and over a grid of 30° by 20°, with about 2.5 s between grid points. The Bentham measured at 310.1, 343.3, and 400 nm on a grid 15° in azimuth by 10° elevation. A total radiance map took about 12 min to complete. The field of view for the Bentham was 1.5° (FWHM) and 3° for the Brewer. These results are discussed in more detail below.

With stability and agreement between instruments confirmed, the schedule for the following days was prepared, as is shown in Table 2. All times are expressed in universal coordinated time (UTC), and local noon was at 1034 UTC. All scans were made in synchronized mode with the time step, and for the wavelength range specified. Instruments that could not complete the full wavelength range stopped at their maximum wave-

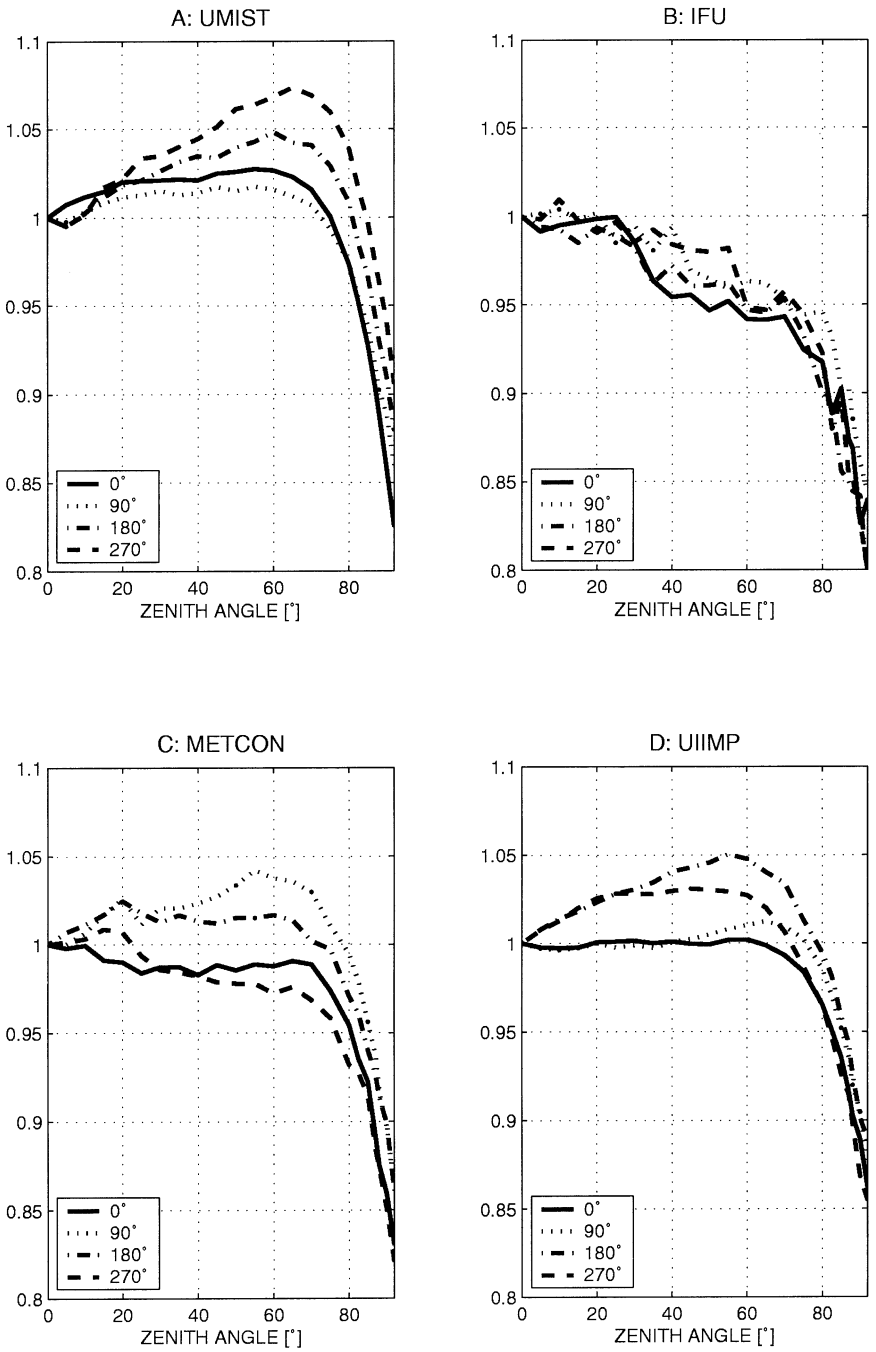

FIG. 1. Angular responses of the actinic heads at 300 nm and across four quadrants (the UIIMP head was not available during the campaign but is used in later ADMIRA work).

length. The radiance distribution measurements could not be fully synchronized but were made at the same times as the other measurements. The two Bentham instruments with both global and actinic capabilities alternated parameters, one measuring actinic on the hour and global on the half hour, while the other took the opposite pattern. Similarly the UIIMP Bentham and Brewer alternated between direct beam and radiance distribution measurements.

The stability checks, thrice daily, for both global and actinic measurements were inserted into the basic schedule. These were times when all instruments capable of making the specified type of measurement (global or actinic) did so. These proved very valuable in confirming that all instruments remained stable throughout the campaign with respect to each other. The wavelength ranges and time steps had to be adjusted to suit the slowest instrument in each group while giving a scan

TABLE 2. The schedule of measurements for each of the full campaign days. The basic schedule (All parameters) is interspersed with stability checks. The time step in parentheses of 1 s was used on 2 of the 6 days (see text for details). The 3-s time step was used for global checks to accommodate the speed of the Brewer.

Time/period (UTC)	Frequency (min)	Scan type	Wavelength range, step (nm)	Time step (s)
0400–0500	30	All parameters	290–500, 0.5	2 (1)
0515		Global check	290–500, 1	3
0530		All parameters	290–500, 0.5	2 (1)
0545		Actinic check	290–400, 0.5	2
0600–0800	30	All parameters	290–500, 0.5	2 (1)
0900–1000	60	All parameters	290–500, 0.5	2 (1)
1030		Global check	290–500, 1	3
1045		Actinic check	290–400, 0.5	2
1100–1300	60	All parameters	290–500, 0.5	2 (1)
1330–1500	30	All parameters	290–500, 0.5	2 (1)
1515		Global check	290–500, 1	3
1530		All parameters	290–500, 0.5	2 (1)
1545		Actinic check	290–400, 0.5	2
1600–1700	30	All parameters	290–500, 0.5	2 (1)

time short enough to fit between the basic schedule measurements. The time steps for the basic schedule were 1 s on 2 days (217 and 219) and 2 s on the remaining days. One second was slightly too fast for the IFU Bentham and resulted in imperfect synchronization, but in the clear sky conditions prevailing it was felt that attempting a faster scan time was worthwhile since it allowed time for additional checks and measurements. Complete measurement sets were obtained on 4–6 August (days 217–219) and 8–10 August (days 221–223). The first three days were completely cloud-free, while the latter three days had some clouds.

The spectral radiation measurements were supported by a wide range of ancillary measurements, in an effort to specify the state of the atmosphere as completely as possible. The supporting instruments are listed in Table 3.

The spectral radiation data, once delivered by the operators, was subject to the National Institute of Public Health and the Environment (SHICrivm) process (Slaper et al. 1995) to correct any wavelength errors in the spectra and map them all onto the equivalent measurement of a virtual instrument with slit width of 1nm FWHM. This has been shown (Webb 1997; Bais et al. 2001) to facilitate the comparison of spectral data from a large number of different instruments by removing well-defined instrument-dependent characteristics from the analysis.

3. Results and discussion

a. Calibration and stability of radiation measurements

The aim of the campaign was to gather a set of directly comparable measurements of different radiation parameters, having first assessed the relative agreement between all the spectroradiometers. The first measurements of global irradiance by the three Benthams and the Brewer, which were independently calibrated using different calibration sources, were in excellent agreement throughout the wavelength range (total range of data was $\pm 4\%$).

On the second day the three instruments with actinic flux and the two with direct irradiance capabilities made their separate intercomparisons. The agreement between the University of Manchester Institute of Science and Technology (UMIST) and IFU actinic fluxes was consistent with both wavelength and solar zenith angle, with a difference between the independently calibrated instruments of about 3% (UMIST $>$ IFU), the same as the global irradiance measurements. In the case of the METCON instrument the signal was noisier than that of the Benthams, giving more high-frequency variation with wavelength in the ratio of two measurements. There was also a diurnal variation of about 10% that appeared when ratioed with either Bentham, and was thus attributed to the METCON instrument. The METCON measurements were in close agreement with the Benthams early and late in the day but measured 10% high when compared with the other two near noon.

An absolute difference of about 9% exists between the direct irradiance spectra measured by the UIIMP Bentham and the Aristotle University of Thessaloniki (AUTH) Brewer (the Brewer measuring higher). However, this difference was consistent to within about 5% during the 6 days of measurements and almost spectrally flat. The reasons for this disagreement were not explicitly identified. Possible causes are differences in the methodology for obtaining the absolute radiometric calibration (either using a lamp or the difference between global and diffuse solar radiation), and effects from the different fields of view (1.5° for the Bentham and 3° for the Brewer).

Comparisons of radiance measurements made by the AUTH Brewer and the UIIMP Bentham revealed that the Brewer measurements are sensitive to light polarization effects. This conclusion is supported by the fact that radiance measurements made with the Brewer at different azimuths while pointing always at the zenith

TABLE 3. Details of the ancillary measurements made to define the atmospheric conditions at the times of the spectral irradiance and acitinic flux measurements.

Instrument	Measured	Schedule
NILU-UV[a] multichannel radiometer	Global radiation at 305, 312, 320, 340, 380 nm, FWHM about 10 nm, and PAR (400–700 nm)	Continuous, 2-Hz, 1-min avgs
NILU cube (suspended)	Global irradiance on six sides at 312 and 340 nm, FWHM 10 nm	Continuous, 2-Hz, 3-s avgs
SL501	Global erythemal UV	0.2-Hz, 1-min avgs
Pyranometer (Eppley)	Total global radiation	0.2-Hz, 1-min avgs
Pyrheliometer (Kipp and Zonen)	Total direct solar radiation	Coincide with scans[b]
Cimel sun photometer	Aerosol optical depth 440, 532, 670, 870, 1020 nm; precipitable water vapor	Coincide with scans[b]
Yankee sky camera	Sky pictures/cloud distribution	Every 15 min
CNR[c] polarization lidar	Aerosol backscatter and extinction at 532 nm. Discrimination solid/liquid/mixed phase of cloud/aerosol types. Observational range 150 m–25 km, resolution 75 m	Coincide with scans[b]
ASASP-X	Aerosol size distribution 0.1–3 μm (roof height sampling)	Continuous, 1-s samples give 1-min avgs
TSI[d] 3653 nephelometer	Backscatter and scattering coefficients at red/green/blue λ (roof height sampling)	Continuous, 1-s samples give 1-min avgs
Brewer Mark III	Column ozone and SO_2	Once or twice per hour depending on schedule of other measurements
Bentham DTM300	Column ozone and aerosol optical depth (from direct scans)	Coincide with scans[b]
Weather station (Conrad Electronic)	Temperature, pressure, humidity, wind speed/direction	Sample every 5 min
Microtops ozone meter (Solar Light)	Column zone and H_2O	Coincide with scans[b]
Ozonesondes	Ozone profile, from airport 10 km distant	Days 218, 219, 223

[a] NILU is the Norwegian Institute for Air Research.
[b] "Coincide with scans" means that the relevant measurements were made once during the period of each scheduled scan.
[c] CNR is the National Research Council.
[d] TSI, Inc.

vary quite significantly, although the photons intercepted by the instrument originate from the same source. In principle, the effect appears as a relative increase of the measured radiance at azimuths perpendicular to the azimuth of the sun. The magnitude of the variation depends on SZA, being ~5% at 24° SZA and increasing to ~40% at 60° SZA. This is consistent with expectations of molecular scattering: a strong polarizer whose effect increases with air mass and is a maximum at 90° scattering angle. The effect of polarization becomes weaker with increasing aerosol content, and this is confirmed by the comparisons to the Bentham measurements over 4 days with different aerosol optical depth. The conclusion is that the radiance measurements attempted with the Brewer instrument are significantly contaminated by polarization effects. This does not affect other measurements made with the Brewer, nor is it an issue with instruments that use a fiber ("scrambling" the spatial pattern of incoming radiation) to deliver radiation to the monochromator (the Brewer uses a prism). The effect is much smaller and within the uncertainties of the measurements only at angles close to the zenith and at high solar elevation angles, especially under conditions of high aerosol optical depth. It remains to be seen whether these measurements can be partially used (e.g., as zonal or total integrals) to extract information on the characteristics of diffuse radiation.

Since agreement during the intercomparisons was so good, the independently calibrated measurements (with the SHICrivm processing) were used in the following presentation of results and could be considered equivalent at the 5% level (wavelengths >304 nm). The observed problems with the Brewer measurements meant that only the direct irradiance and radiance distributions from the Bentham instrument could be used in analysis.

Figure 2 shows the global irradiance and actinic flux stability checks from day 222. All ratios are made with the UMIST instrument (which measured both actinic flux and irradiance) as denominator and computed from the spectral data after SHICrivm analysis. The high-frequency structure is characteristic of the ratios of any pair of instruments. It is due to the different slit functions of the instruments and their effects on the individual measurements of the Fraunhofer structure of the sun's spectrum. Much of the effect is removed by the SHICrivm procedure, but a residual structure remains. Figure 2a shows that all instruments measured global irradiance within ±5% of each other throughout the day. The UIIMP/UMIST ratio was very stable during the day, while the AUTH Brewer decreased in sensitivity relative

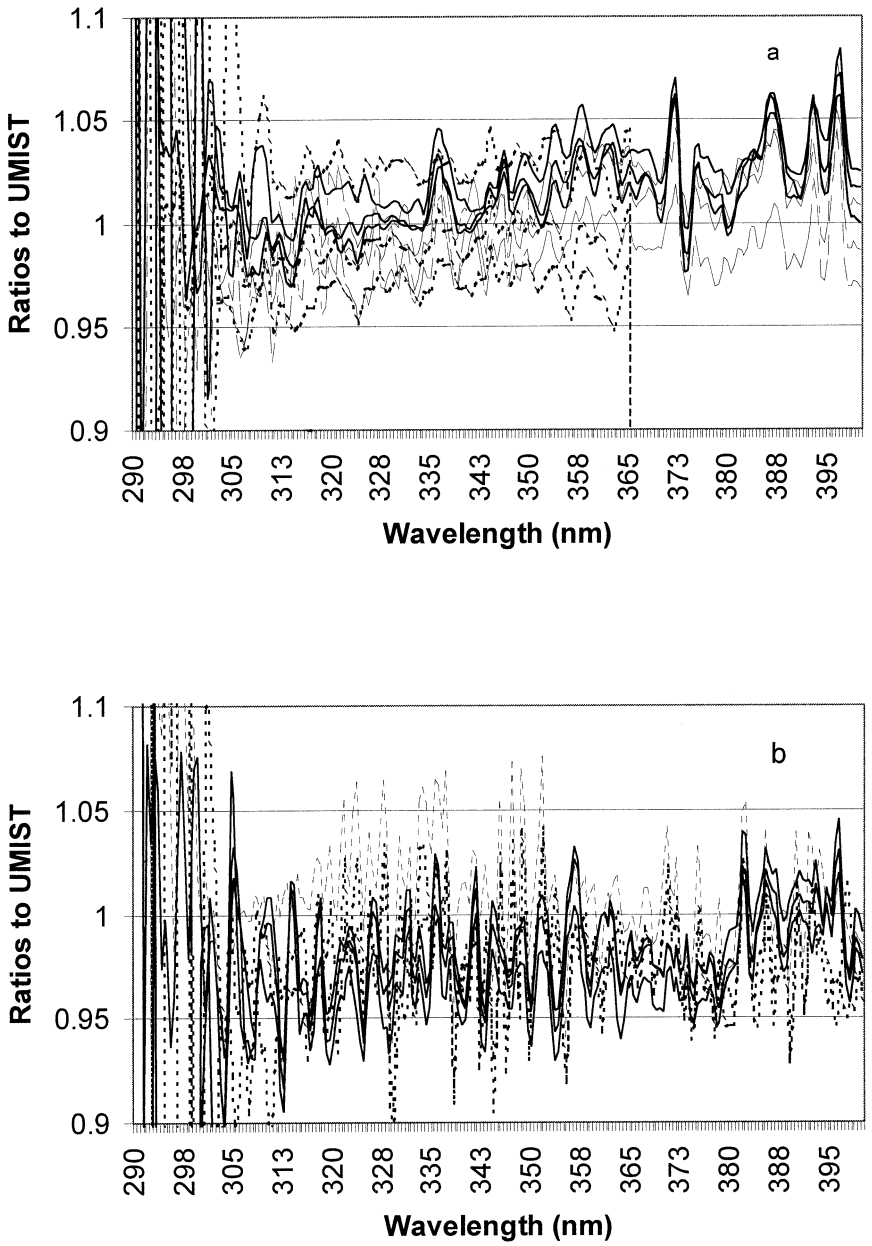

FIG. 2. Results of the three stability checks on day 222 expressed as a ratio of each instrument to the UMIST measurement for (a) global irradiance at SZA of 71°, 24°, and 64° (UIIMP, solid lines; AUTH, dotted lines; IFU, dashed lines) and (b) actinic flux at SZA of 66°, 24°, and 70° (IFU, solid lines; METCON, dotted lines).

to the other instruments, but remained within the total measurement range above. The total variation in actinic flux measurements (Fig. 2b) is similar at ±5%, although the ratios have more structure and a mean value of about 0.98. This suggests that the UMIST instrument was measuring about 2% higher than the IFU instrument. The METCON spectroradiometer had a diurnal dependency to its absolute measurements, and much, but not all, of the noise in Fig. 2b is also attributed to the METCON instrument. The stability checks shown were made one week after the instruments were initially calibrated and installed, and because very similar results were obtained on all days of the campaign it is possible to state the 5% equivalency given above. This stability also applies to the direct irradiance measurements.

b. Atmospheric conditions during the campaign

The aim of the campaign was to explore the relationship between global irradiance and actinic flux in a

well-specified atmosphere. The state of the atmosphere was defined by the ancillary measurements.

Conditions throughout the campaign were fairly stable, with consistent diurnal patterns in temperature, wind direction, and associated parameters. Pressure throughout the campaign was in the range 1005–1014 hPa. The diurnal temperature range was about 6°C, and the wind was offshore during the morning, swinging round to onshore in the afternoon as the sea breeze set in. Column ozone, as measured by direct sun observations of the Brewer (uncertainty ±1%), increased gradually through the campaign. Unfortunately, no ozonesonde exceeded a height of 18 km, so for the higher-level ozone profile, data from the Global Ozone Monitoring Experiment (GOME) have been used (Van der A et al. 1998). The Brewer also indicated that there was negligible SO_2 in the atmosphere.

Aerosol information was available from a variety of sources. Sampling of near-surface air by the Active Scattering Aerosol Spectrometer Probe (ASASP-X) gave aerosol size distribution (±10%) while the nephelometer provided total backscatter and scattering coefficients representative of the lower boundary layer. The ASASP-X measures He–Ne laser light scattered by particles drawn through the laser beam. Scattering is a direct function of particle size, and a pulse height analyzer thus separates the aerosol into size channels between 0.1 and 3.0 μm. The nephelometer, sampling air at the same height, measured back- and total scattering coefficients at three wavelengths in the red, green, and blue spectral ranges. The tropospheric lidar provided profile information up to the tropopause for backscatter and extinction coefficient at 532 nm and depolarization from which aerosol and cloud phase can be inferred. Aerosol optical depth [AOD; described by Ångstrom (1961) as $\tau_{a\lambda} = \beta\lambda^{-\alpha}$ where α is the wavelength exponent associated with the aerosol size distribution and β is Ångstrom's turbidity coefficient] at a number of wavelengths (e.g., 350 nm) could be derived from direct sun spectral measurements (uncertainty ±0.05), while the Cimel sun photometer provided AOD at 440, 532, 670, 870, and 1020 nm. At 440 nm, where both instruments were measuring, the absolute agreement in AOD was better than 0.1. The lidar-estimated and Cimel-measured AOD at 532 nm also agreed well.

The Ångstrom–alpha coefficient was derived from the direct sun spectra. Precipitable water in the column was also available from a handheld Microtops instrument and from the Cimel channel at 940 nm that was validated against the radiosoundings from Thessaloniki, Greece.

Aerosol optical depth and precipitable water vapor (PWV) followed similar patterns. Both were lowest in the first three days, with minima on day 218. The radiosoundings show a well-mixed and fairly moist layer from the ground to about 700 hPa (about 3100–3200-m altitude), with a drier atmosphere above. Values then increased to maxima on day 223, with the atmosphere now moist up to 600 hPa (about 4300–4400-m altitude). The decreasing Ångstrom coefficient indicated an increase in larger particles when the AOD increased.

Looking at the ground-based ASASP-X data (1-min averages of particle numbers with an estimated uncertainty of 10%) there was a distinct and consistent aerosol size distribution in the lower boundary layer. Day 218 had lowest particle concentrations, although there were no dramatic changes in low-level aerosols during the campaign. During the measurement period (0400–1700 UTC) aerosol loading remained fairly constant on all days, sometimes with a slight decline during the day, especially after the sea breeze began.

The nephelometer was sampling the same lower boundary layer air as the ASASP-X but, in contrast to particle numbers, the scattering coefficients show a strong diurnal variability, indicating advection, temperature, and boundary layer mixing processes. There was generally a sharp peak in scattering coefficient between 0400 and 0800, followed by a more or less constant scattering for the remainder of the measurement period. Only the last two days of the campaign, after an airmass change, did not show this characteristic feature, with fairly constant scattering throughout the day.

At higher levels details of the aerosol properties come from the VELIS and again show no dramatic change in conditions, though there were significant differences in the profiles from day to day (Fig. 3). During the first three days, low aerosol optical depth (AOD = 0.1–0.3 at 532 nm) was associated with an aerosol layer mainly confined below 3 km, and depolarization values indicated that most of the backscatter was generated by spherical (i.e., liquid) particles (Gobbi et al. 2000). An increasing aerosol load characterizes the second period of measurements (days 221–223), but with no substantial variation in the aerosol type. Liquid cloud formation was first observed on day 222, with more and more variable (liquid and ice) clouds on day 223.

The remainder of the ancillary instruments provided supporting radiation data. In conjunction with the Yankee sky camera, they helped to identify the influence of clouds by, for example, giving the direct and diffuse partitioning of total solar radiation. In addition, continuous series of measurements were available throughout the day for total solar radiation, erythemally effective radiation, narrow band radiation centered at 305, 312, 320, 340, and 380 nm and photosynthetically active radiation (PAR). From these, the time and extent of deviations from the ideal clear-sky curve could be identified for each waveband.

During the first three days (217–219) of the full campaign, no clouds were observed by the personnel on site or the sky camera. The latter days (221–223) brought varying amounts of cloud, but only the final day (223) began with no direct sun (cirrus and stratus cover). Clearly identifiable cloud disappeared during the morning, but the direct sun was still visibly reduced either by very thin cirrus or aerosols.

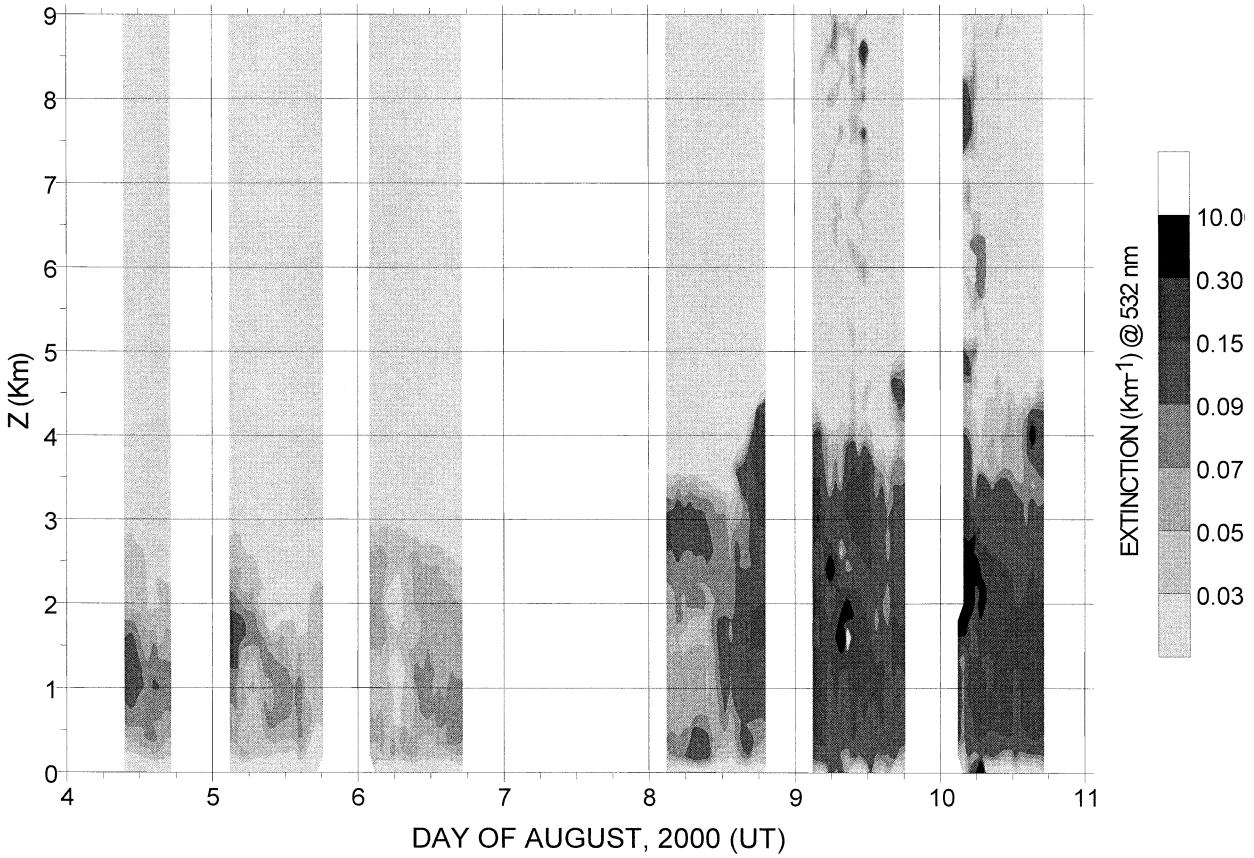

FIG. 3. VELIS profiles: contour plot of the lidar-derived aerosol extinction profiles (532 nm) during the ADMIRA campaign. Inversion has been performed by means of a continental aerosol model and was validated against sun photometer observations.

The two days with most contrast, judged from aerosol and cloud observations, are used to investigate the radiation fields. They were day 218 (5 August) and day 223 (10 August). On day 218 there were no clouds, the campaign minimum optical depth was reached in the afternoon, and most of the aerosols were below 2000 m. Surface aerosol was also the minimum for the campaign. By contrast, day 223 had aerosols up to 6 km, morning cloud between 6 and 9 km and maximum aerosol optical depths. In the afternoon there was no cloud until about 1500 UTC, when some nucleation was observed, almost at the end of the measurement period. See Fig. 4 for the prevailing conditions on each day.

c. Global irradiance and actinic flux

Figure 5 shows the spectra of actinic flux F and irradiance E, measured by UMIST and IFU, respectively, at 0500 and 1000 UTC on day 218. The detailed comparison of global irradiance and actinic flux is presented as the ratios (F_{UMIST}:E_{IFU}) measured on the full hour. Measurements were also made on the half hour, with each instrument measuring the opposite parameter, but for clarity of presentation, and to retain a consistent ratio, only the hourly data are used. There was a consistent 2%–3% difference between the calibrations of these two instruments, giving a systematic 2% overestimation in every ratio. In addition, the stability checks showed diurnal variations between the two instruments of no more than $\pm 1\%$ at all wavelengths, and a high-frequency wavelength-dependent structure of $\pm 5\%$ (peak-to-trough extremes). The maximum uncertainty is therefore 3% in the smoothed ratios and 7% at a specified wavelength.

The ratios $F:E$ as functions of wavelength and time are presented in Figs. 6 and 7 for days 218 and 223, respectively. Note that local solar noon was at 1034 UTC so the hourly measurements are not completely symmetrical about solar noon.

In Fig. 6 (top) it is seen that at an SZA of less than about 40° the $F:E$ ratio is virtually independent of wavelength, and, as SZA increases, it increases from about 1.4 (SZA = 24°) to 1.6 (SZA = 40°). At SZA $> 50°$, the ratios show an increasing, linear, wavelength dependency. The $F:E$ ratio continues to increase at UVB wavelengths, to a maximum of about 1.8 at SZA = 85°, but the ratios are far greater approaching the visible: 2.6 at SZA = 72.7° and a wavelength of 400 nm. Figure 6 (bottom) gives a clearer representation

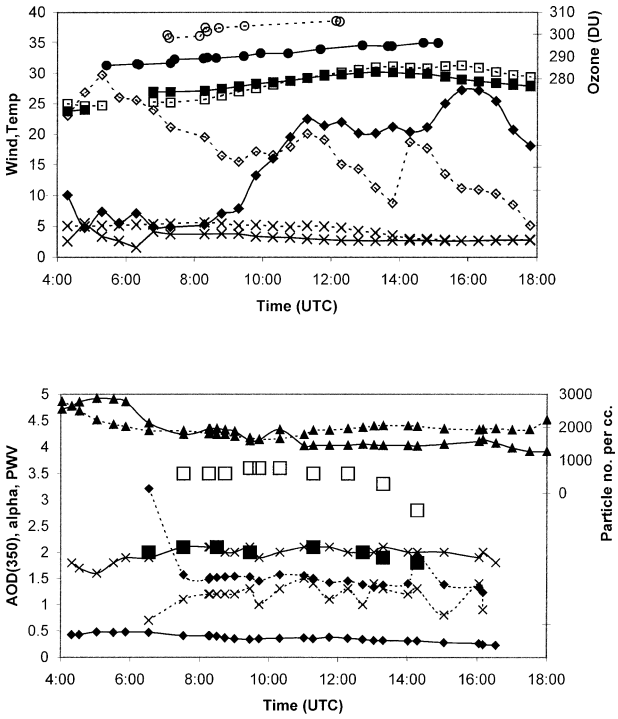

FIG. 4. Atmospheric conditions on days 218 and 223. Solid lines are day 218, dotted lines are day 223. (top) Ozone (circles), temperature (°C; squares), wind speed (m s^{-1}; diamonds), and wind direction (rad; crosses). (bottom) Particle number (triangles), aerosol optical depth (diamonds), alpha coefficient (crosses), and precipitable water vapor (cm; large squares: solid day 218, open day 223).

of the diurnal change in the $F:E$ ratio at different wavelengths. The peak value of the ratio is higher and occurs earlier/later in the day at 400 nm than at shorter wavelengths.

Exploring the $F:E$ ratios at wavelengths longer than 400 nm introduces greater uncertainties, since only two instruments measured the required data to 500 nm; so the slightly less stable METCON data had to be used, and no SHICrivm analysis was available. The data are also less relevant to photolysis rates than the UV wavelengths. Nonetheless, a brief description follows for day 218 for which there were no complications of cloud and least aerosol. The investigation is restricted to the basic data (no SHICrivm analysis available) of $F_{\mathrm{METCON}}:E_{\mathrm{UMIST}}$ at measurements made 30 min past each hour. The relative calibrations of the two instruments were assessed to give an overall uncertainty in the trend of the $F_{\mathrm{METCON}}:E_{\mathrm{UMIST}}$ ratio in the visible of 6% of the ratio.

The $F:E$ ratios for the two times closest to the extremes of behavior in the UV were calculated: 0530 UTC (greatest wavelength-dependent increase in UV) and 1030 UTC (no wavelength dependency in UV). At 0530 UTC the ratio showed no real wavelength dependency in the visible, staying at an almost constant value of about 2.25. At 1030 UTC, when the ratio is essentially constant in the UV, it decreases steadily through the visible part of the spectrum, from 1.4 at 400 nm to 1.15 at 500 nm, a pattern consistent with the leveling of the ratio at 0530. The minimum ratio at visible wavelengths is thus in the middle of the day, as for UV, and increases as SZA increases, but the wavelength region around 400 nm appears to be the pivotal point about which the wavelength dependency of the ratio can change.

The UV data for day 223 (10 August) are shown in Fig. 7. It is immediately apparent that the range of the $F:E$ ratio is much reduced and that there is less wavelength dependency to the ratios. Away from the noon hours the ratios increase slightly through the UVB but then remain essentially constant above 340 nm, in con-

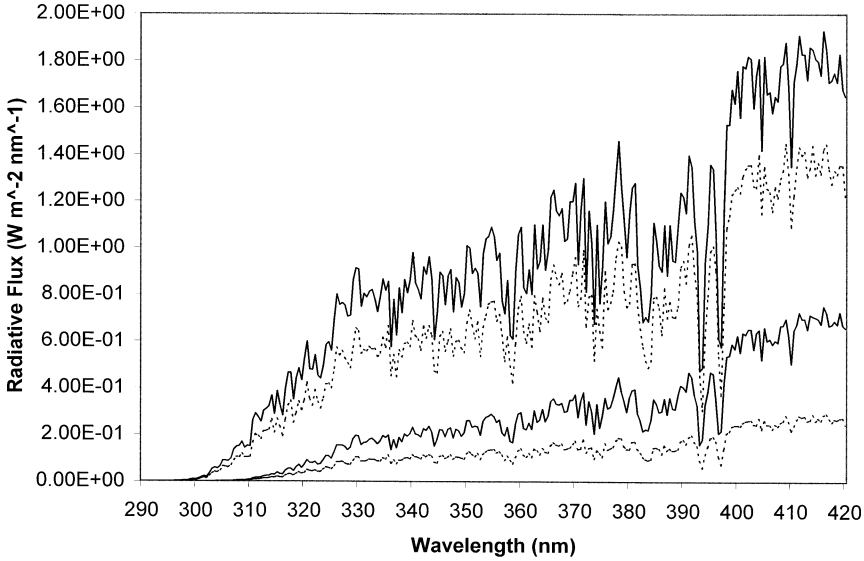

FIG. 5. Absolute values of irradiance (dotted line) and actinic flux (solid line) at 0500 and 1000 UTC on day 218.

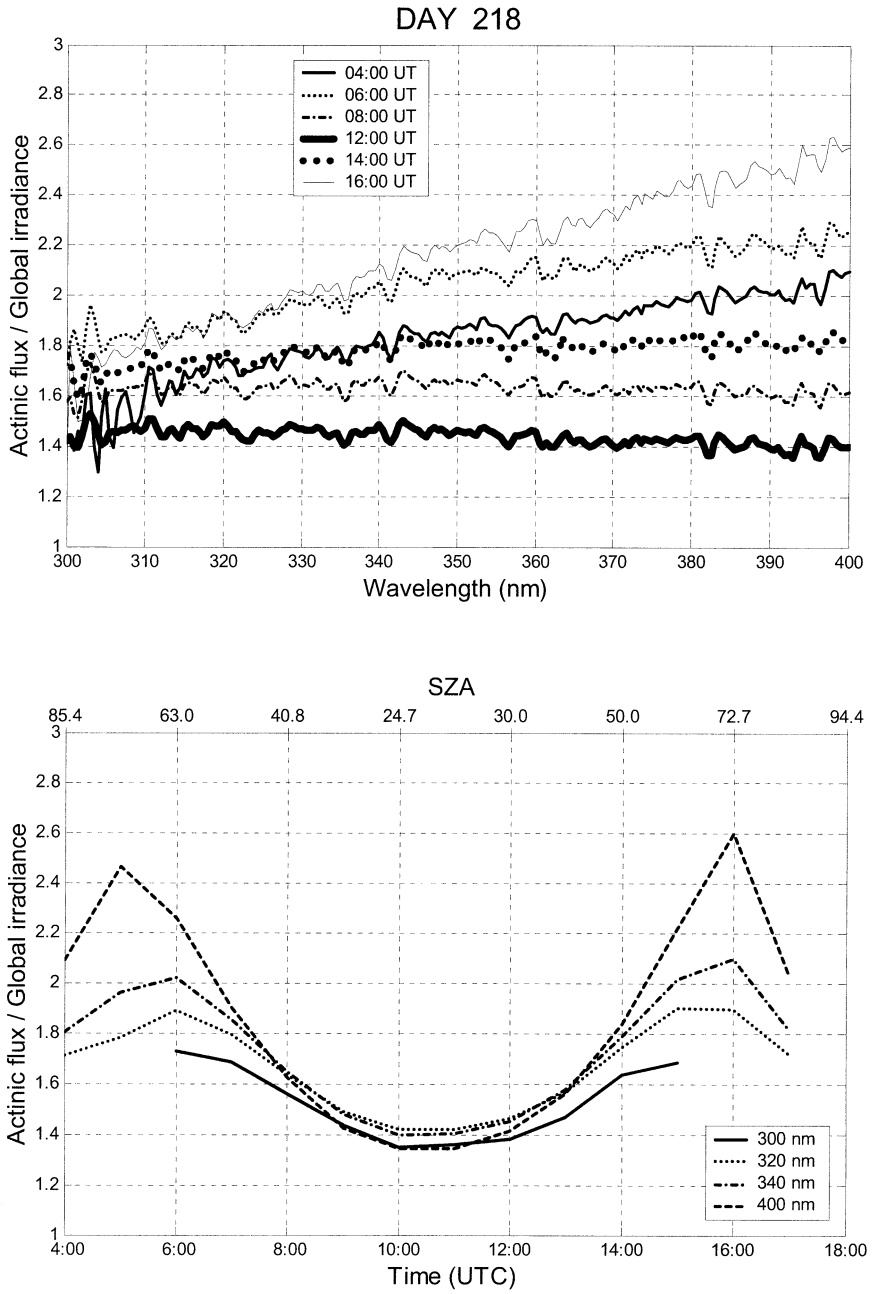

FIG. 6. The $F:E$ ratio for day 218 as a function of wavelength at different times (top) and as a function of time at selected wavelengths (bottom).

trast to the continuing increase with wavelength on the clearer day. The diurnal pattern of ratios [Fig. 7 (bottom)] is more asymmetrical than in Fig. 6 (bottom), reflecting the bigger differences in atmospheric conditions between morning and afternoon on day 223. The underlying pattern of a midday minimum with midmorning and afternoon maxima remains but is less pronounced than under clear conditions. The maxima are also at the same times (0700 and 1500) for all wavelengths, instead of being earlier/later at longer wavelengths as on day 218.

These results are within the range of those expected from previous work, and model calculations made for the site in Nea Michaniona before the campaign. Clearly the spectral measurements give more detail than broadband data (Van Weele et al. 1995) and are measured, not simulated [see Kazadzis et al. (2000), or our own simulations], thus providing more information

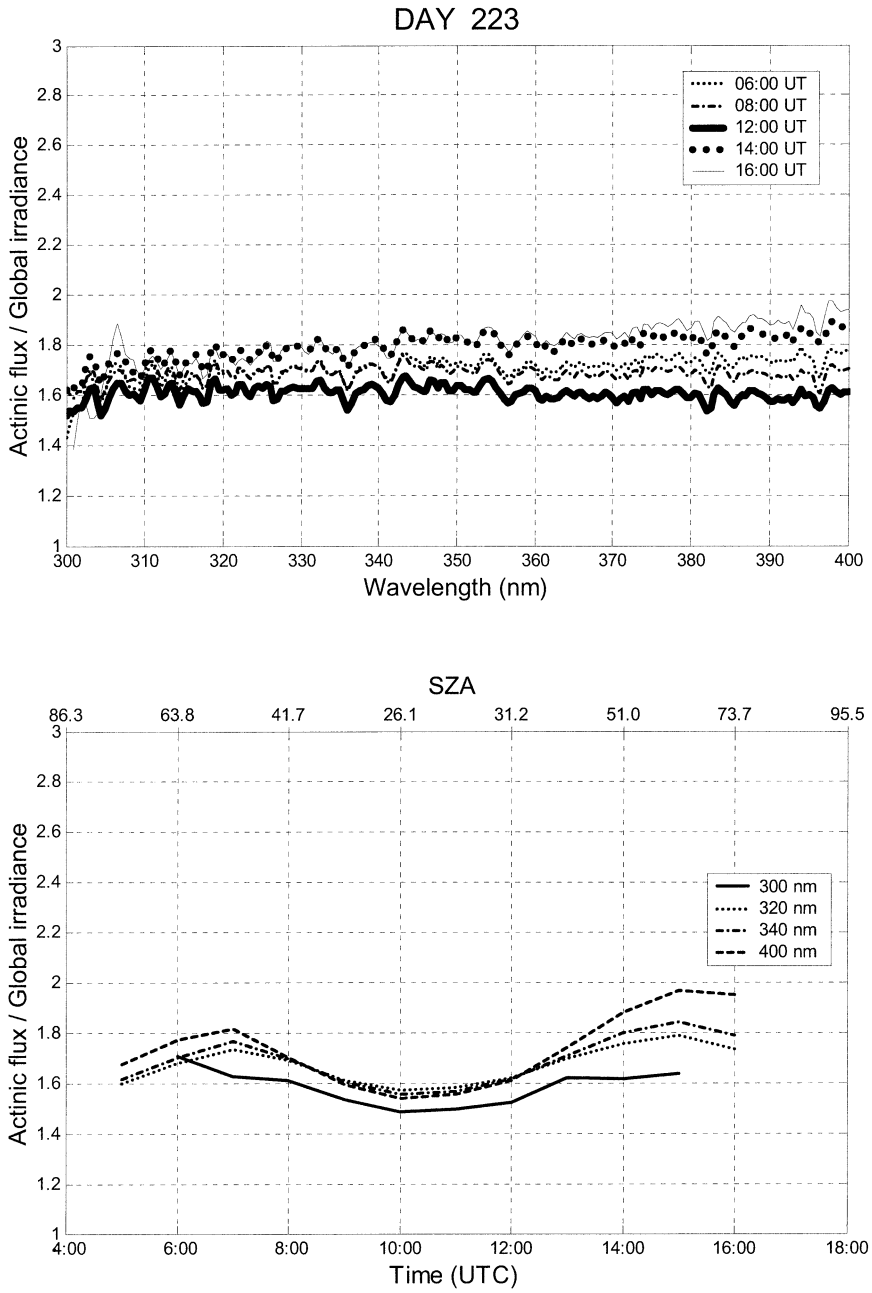

FIG. 7. Same as Fig. 6, but for day 223.

about radiation in a real atmosphere while confirming the more generalized broadband and simulated information.

The ratio of actinic flux to global irradiance is strongly dependent on the amount and isotropy of scattering in the atmosphere. In terms of other radiation parameters measured it depends on the direct–diffuse partitioning of the radiation and the radiance distribution. These in turn depend upon wavelength, SZA (pathlength), and the amount of scatterers along the pathlength. In a clean, clear atmosphere Rayleigh scattering dominates and has a λ^{-4} dependency, while scattering by aerosol and cloud particles have a comparatively smaller dependence on wavelength. The ratios of direct/global irradiance for days 218 and 223 are shown in Fig. 8 for an SZA of 47°. There is a clear difference between the days. The direct contribution to global irradiance on day 223 is half that on day 218, while at 320 nm the change from one day to the other is a factor of 3. The increased scattering on day 223 is also apparent in the sky radiance distributions. This is illustrated by two representative values, the minimum radiance on the hemisphere (usu-

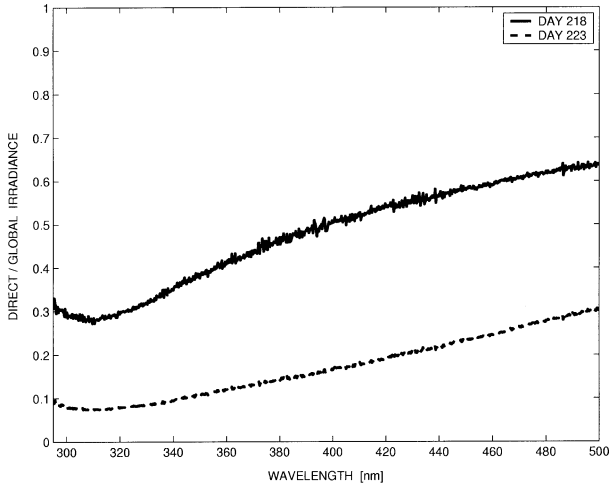

FIG. 8. Direct/global irradiance measurements for days 218 and 223 at a solar zenith angle of 47°.

ally about 80° from the sun, excluding the horizon), and the ratio of the radiances at 5° and the minimum value. An example is given for midafternoon (SZA = 57°). The ratio is between 3.2 (310 nm) and 9.8 (400 nm) on day 218, while corresponding values for day 223 are 2.3 and 6.4. The higher AOD and more scattering on the latter day decreases the contrast between the circumsolar and sky radiation. Further evidence of the increased scattering and more homogenous radiance distribution on day 223 comes from the minimum radiances, which were higher on day 223 than on day 218 at 343 nm (0.0422–0.0340) and 400 nm (0.0552–0.0356). At 310 nm the absolute values are dominated by the differences in ozone on the two days and are thus marginally lower on day 223.

4. Conclusions

The ADMIRA campaign has provided a unique dataset of spectral UV irradiance and actinic flux measurements supported by a comprehensive set of ancillary data to define the atmospheric conditions at the time of measurement. In so doing the experiment also confirmed the absolute agreement and stability of several instruments measuring irradiance, and established similar properties among instruments making actinic flux measurements for the first time. Comparisons of direct irradiance measurements highlighted the discrepancies in absolute calibration that can arise from different calibration methods (laboratory or global − diffuse solar radiation). A polarization problem was also identified in the Brewer spectrophotometer, invalidating efforts to measure radiance distribution with this instrument.

The data have been used to illustrate the $F:E$ ratio on two contrasting days. This shows that both the wavelength dependency and the SZA dependency of the ratios decrease as the scattering in the atmosphere increases. In general, the ratio increases with wavelength in the UV but then plateaus or begins to decrease at visible wavelengths. Both the wavelength dependency and the absolute values of the ratio increase as SZA increases, to a maximum at 50°–60° SZA (wavelength and aerosol dependent), and thereafter decrease.

These data will be further used to develop algorithms to convert spectral UV irradiance data to spectral actinic fluxes, hence enabling the calculation of photolysis rates wherever spectral UV irradiance data are available. The algorithms will be tested on sets of synchronized irradiance and actinic flux data from several different monitoring sites with varying conditions and climates as the next phase of the ADMIRA program.

Acknowledgments. The participants of the ADMIRA campaign (Project EVK2-CT-1999-00018) would like to express their appreciation to the director and the staff of the Academy of Mercantile Navy of Macedonia, for hosting the campaign and for providing all the available facilities at Nea Michaniona. We thank the European Community for funding this work within the Fifth Framework Programme, and the staff of the Laboratory of Atmospheric Physics at the University of Thessaloniki for all their work as local organizers.

REFERENCES

Ångstrom, A., 1961: Technique of determining the turbidity of the atmosphere. *Tellus,* **13,** 214–223.

Bais, A. F., and Coauthors, 2001: The SUSPEN intercomparison of ultraviolet spectroradiometers. *J. Geophys. Res.,* **106,** 12 509–12 525.

Gobbi, G. P., F. Barnaba, R. Giorgi, and A. Santacasa, 2000: Altitude-resolved properties of a Saharan dust event over the Mediterranean. *Atmos. Environ.,* **34,** 5119–5127.

Hofzumahaus, A., A. Kraus, and M. Muller, 1999: Solar actinic flux spectroradiometry: A new technique to measure photolysis frequencies in the atmosphere. *Appl. Opt.,* **38,** 4443–4460.

——, ——, A. Kylling, and C. Zerefos, 2002: Solar actinic radiation (280–420 nm) in the cloud-free troposphere between ground and 12 km altitude: Measurements and model results. *J. Geophys. Res.,* in press.

Kazadzis, S., A. F. Bais, D. Balis, C. Zerefos, and M. Blumthaler, 2000: Retrieval of downwelling UV actnic flux density spectra from spectral measurements of global and direct solar UV irradiance. *J. Geophys. Res.,* **105** (D4), 4857–4864.

Madronich, S., 1987a: Intercomparison of NO_2 photodissociation and UV radiometer measurements. *Atmos. Environ.,* **21,** 569–578.

——, 1987b: Photodissociation in the atmosphere. 1: Actinic flux and the effects of ground reflection and clouds. *J. Geophys. Res.,* **92,** 9740–9752.

McKenzie, R. L., P. Johnston, A. Hofzumahaus, A. Kraus, S. Madronich, C. Cantrell, J. Calvert, and R. Shetter, 2001: Relationship between photolysis frequencies derived from spectroscopic measurements of actinic fluxes and irradiances during the IPMMI campaign. *J. Geophys. Res.,* in press.

Nader, J. S., and N. White, 1969: Volumetric measurement of ultraviolet energy in an urban atmosphere. *Environ. Sci. Technol.,* **3,** 849–854.

Shetter, R., and M. Mueller, 1999: Photolysis frequency measurements using actinic flux spectroradiometry during the PEM–Tropics mission: Instrumentation description and some results. *J. Geophys. Res.,* **104,** 5647–5561.

Slaper, H., H. A. J. M. Reinen, M. Blumthaler, M. Huber, and F. Kuik, 1995: Comparing ground level spectrally resolved UV mea-

surements using various instruments: A technique resolving effects of wavelength shift and slit width. *Geophys. Res. Lett.*, **22,** 2721–2724.

Van der A, R. J., R. F. van Oss, and H. M. Kelder, 1998: Ozone profile retrieval from GOME data. *Satellite Remote Sensing of Clouds and the Atmosphere III*, J. E. Russell, Ed., *Proc. SPIE*, **3495,** 221–229.

Van Weele, M., J. V.-G. de Arrelano, and F. Kuik, 1995: Combined measurements of UV–A actinic flux, UV–A irradiance and global radiation in relation to photodissociation rates. *Tellus*, **47B,** 353–364.

Webb, A. R., 1997: Advances in solar ultraviolet spectroradiometry. Air Pollution Research Rep. 63, Office for Official Publications of the European Communities, Luxembourg, 238 pp.